Surface Tension, Density and Composition in the Methane-Pentane System at High Pressure

John Satherley,* David L. Cooper and David J. Schiffrin

Department of Chemistry, University of Liverpool, Liverpool, L69 7ZD, U.K.

ABSTRACT: A pressure system is described for measuring the pressure dependence of surface tension using digital image processing techniques on pendant drops in systems where the miscibility changes with both temperature and pressure. Measurements can be performed at pressures up to 40 MPa and temperatures up to 423 K. This high-pressure rig allows, additionally, the simultaneous measurement of both phase density and composition. The system is tested with the methane-pentane system at 313.15 K and pressures up to 15.6 MPa; the results compare well with literature data and with values calculated using the Peng-Robinson equation of state in conjunction with the gradient theory approach to computing surface tension, thus validating the experimental technique. Density profiles of the components through the interfacial layer have also been calculated using gradient theory. The Wegner extended scaling approach has been applied to all of the data sets to estimate the critical pressure for this system, which is found to be 16 MPa at 313.15 K.

1. INTRODUCTION

Pressure effects on physicochemical properties continue to be the subject of a great deal of research not only in the physical sciences [1, 2] but recently also in food science [3, 4]. There are practical and fundamental reasons for this: many chemical reactions and processes are carried out at high pressure [5] and, also, measurements under pressure are a simple and convenient way to study properties of condensed media that are dependent on the average molecular separation in the fluid. Furthermore, the need for improved oil recovery [6] has led to the study of pressure effects on aqueous-hydrocarbon systems with added surfactants and on miscible systems close to a critical point [7].

Surface tension (liquid/vapor) or interfacial tension (liquid/liquid), due to their influence on capillary forces in porous media, are important parameters for petroleum reservoir simulation [8, 9]. For accurate predictions of oil recovery, surface tension data at reservoir conditions are required. However, there is still a significant paucity of data on surface tension under extreme conditions that are suitable for testing scaling and extended scaling theories of criticality, especially for highly miscible liquid/liquid and liquid/gas systems. These are all important considerations for the efficient use of existing resources in a period requiring a decreasing reliance on fossil fuels and an increasing decarbonization of energy production, as well as for the possibility of CO_2 sequestration in reservoirs that are out of production. Furthermore understanding the phase behavior and fluid surface properties of reservoirs that exhibit retrograde behavior, such as Eagle Ford [10] in southern Texas, are becoming increasingly important in this transitional period.

The present work combines an experimental approach for measuring surface tension under pressure with theoretical analysis of surface tension and of density profiles. Equipment is described that is designed to operate at pressures up to 40 MPa and temperatures up to 423 K. It is capable of making measurements of surface tension down to the ultralow region ($\sim 1 \times 10^{-3}$ mN m^{-1}) [11] and of phase densities and compositions for highly miscible systems. Surface tension is determined using the Laplace-Young equation applied to the profile coordinates of a pendant drop, as acquired by video image processing. The central purpose of this work is thus to validate the experimental approach by a comparison of the data with existing literature data and theoretical predictions.

The most frequently used method to determine surface tension under elevated pressure conditions is the pendant drop technique. Hauser and Michaels [12] were the first to construct a high-pressure cell enabling surface tension to be measured at pressures up to 66.7 MPa and

temperatures up to 473 K. Their high-pressure cell was filled with a fluid, *A*; a drop forming injector, sealed into the top of the pressure cell, had its tip immersed in fluid *A*. By gently forcing a second fluid, *B*, through the injector, a droplet of fluid *B* surrounded by fluid *A* was formed at its tip. Windows on opposite sides of the cell allowed the drop to be photographed and subsequently analyzed by the selected plane method [13, 14] to determine the boundary tension.

This basic design has been used with small improvements by various groups. Hough, Rzasa and Wood [15] enhanced the design so that samples could be injected without contacting either air or mercury. A further modification [16] to measure liquid/gas surface tension was to fill the body of the cell with liquid and to form a gas droplet on the injector tip. Jennings [17] included a tip holding turret that permitted five tips to be rotated into position under pressure. This feature obviated the cumbersome task of taking the system apart when the surface tension became too low to form analyzable drop shapes with a given tip diameter.

The experimental arrangements just described work well for immiscible or near immiscible systems. However, for systems which change miscibility with temperature or pressure, the liquids must first come to thermodynamic equilibrium inside the pressure container before a droplet of one fluid is formed in another. The new high-pressure rig described in the present work addresses this important problem, which is relevant to a range of applications, including enhanced oil recovery.

There are of course other ways of determining surface tension at high pressure such as laser light scattering [18-21], capillary rise [22] and maximum bubble pressure [23] techniques. However, for nearly miscible systems there are disadvantages with all of these techniques. Wetting and contact angles need to be taken into account in the capillary rise technique. Easily renewing the liquid surface is very difficult with the laser light scattering technique and measuring very low values of surface tension with the maximum bubble pressure and capillary rise techniques is difficult. All of these issues become increasingly important as surface tension decreases towards very low values.

New experimental data are reported here for the densities and compositions of the phases and for the surface tension of the methane-pentane system at a temperature of 313.15 K. These results are compared with values calculated using the Peng-Robinson equation of state and gradient theory. In addition we have used Wegner's extended critical scaling theory [24] to determine the critical pressure of the binary methane-pentane system at this temperature. The critical pressure has then been used to examine the scaling of surface tension and of density difference with the reduced pressure, and with each other.

2. EXPERIMENTAL AND COMPUTATIONAL DETAILS

2.1. Experimental. A high-pressure cell was constructed (see Fig. 1) so as to allow the bulk liquid and vapor phases to reach equilibrium and then, secondly, for a pendant drop of the liquid phase to be formed in the vapor phase. In this way, a fresh surface can easily be formed and the liquid phase forming the pendant drop is in equilibrium with the surrounding vapor phase. All of the apparatus is linked together in the high-pressure rig shown schematically in Fig. 2. The cell and optical system are mounted on an anti-vibration table to minimize disturbance to the pendant drops, which are viewed through optical windows. Fluids are moved around the rig with a circulating pump. The rig was specifically designed so that measurements can be performed at pressures up to 40 MPa and temperatures up to 423 K.

Liquid and vapor phase densities are measured using an Anton Paar DMA 512 high-pressure densitometer coupled to an Anton Paar DMA 55. The densitometer was calibrated as a function of pressure (0.1 to 40 MPa) using Milli-Q grade (resistivity 18.2 MΩ cm at 25°C) degassed water and helium (BOC, 99.999 mol%) at a temperature of 313.15 K. The densities of water and helium were taken from Refs. [25] and [26], respectively.

The composition of each phase is measured by gas chromatography using an ATI Unicam 4600 with thermal conductivity as the detection method and helium as the carrier gas. This instrument is fitted with a 5 m column (mesh size 60-80, liquid phase DC200/350, absorbent support Chromosorb P) and is capable of separating hydrocarbons from methane to decane. The input to the column from the high-pressure rig is via a Valco high-pressure (35 MPa) injection valve containing a sample loop with a volume of 0.5 μL. The number of moles of each component in a mixture was taken as the ratio of the gas chromatography peak areas of that component in the mixture to that of the pure component (at identical conditions as in the mixture).

The temperature is measured in several locations in the rig using class A platinum resistance thermometers which conform to the IEC 751:1983 standard on the 1968 temperature scale and a Phillips DVM type PM 2534 is used to measure the resistance. The pressure in the rig is measured with a Budenberg Standard Test Gauge (dial diameter 250 mm, pressure range 0.1 to 70 MPa, smallest division 0.5 MPa) which had been calibrated by the manufacturer using a deadweight pressure balance: a certificate verifying this calibration accompanied the gauge when it was purchased.

The specifications and sources of the methane and *n*-pentane used in the high-pressure rig are reported in Table 1 along with the purity levels stated by the suppliers. These chemicals were used as received, without further purification.

Table 1. Specifications and sources of the alkanes used in the high-pressure rig.

Chemical	Stated purity (mol %)	Supplier
methane	99.995[a]	BOC
n-pentane	>99.5[b]	Fluka

[a] Impurities stated by BOC: $O_2 \leq 5$, $N_2 \leq 20$, $H_2 \leq 5$, other hydrocarbons ≤ 20, and $H_2O \leq 5$ (in ppm). [b] Gas chromatography analysis as stated by the supplier.

The digitized video image method of acquiring profile coordinates that has previously been described [27] was used with the addition of a powerful photomacrographic lens. Surface tension was calculated using the complete set of profile coordinate data fitted to drop shapes generated by the Laplace-Young equation. Briefly, these drop shapes can be expressed by a set of three first-order differential equations:

$$\frac{dx}{ds} = \cos \phi$$

$$\frac{dz}{ds} = \sin \phi$$

$$\frac{d\phi}{ds} = 2 + \beta z - \sin \frac{\phi}{x}$$

$$(1)$$

in which all of the symbols are indicated in Fig. 3a except for β, which is the drop shape parameter given by:

$$\beta = \frac{\Delta \rho g r_0^2}{\gamma}$$

$$(2)$$

where $\Delta \rho$ is the measured bulk density difference between coexisting phases, g is the acceleration due to gravity, r_0 is the radius of curvature at the drop apex and γ is the surface tension.

Fig. 1 Schematic diagram of the high-pressure surface tension cell.[a]

[a] Dimensions (length × diameter) of pressure vessel body: external 292 mm × 127 mm, internal 200 mm × 50.8 mm. KEY: 1. Syringe plunger manipulator; 2. Syringe barrel manipulator; 3. Tommy-bars for fine control of manipulators; 4. Closure plug; 5. Closure head; 6. Pressure vessel body; 7. Dynamic Viton 'O'-ring seals; 8. Spacer to reduce internal volume; 9. High-pressure gas port; 10. Platinum resistance thermometer port; 11. Syringe plunger; 12. Syringe mounting assembly; 13. Locking screws; 14. Syringe barrel; 15. Window assembly; 16. Liquid phase; 17. Vapor phase.
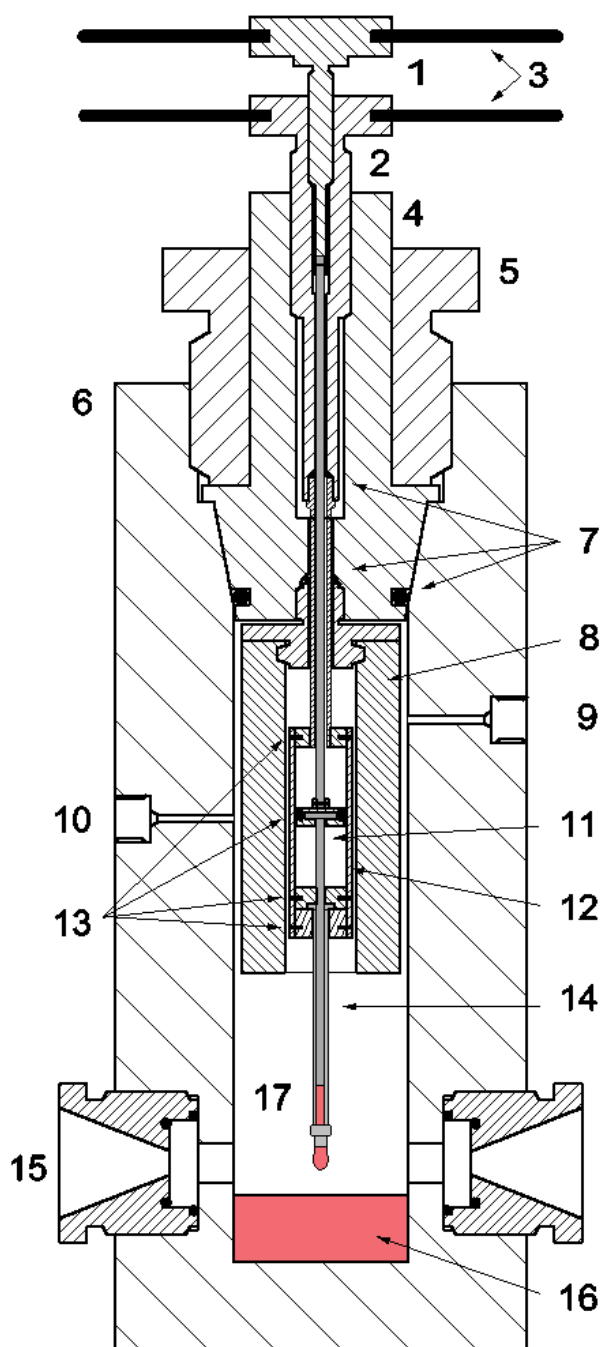
Fig. 2 Schematic diagram of the high-pressure rig.[a]

[a] KEY: 1. Digital readout from platinum resistance thermometers; 2. Water bath; 3. High-pressure surface tension cell (Fig. 1), 4. Pendant drop syringe; 5. Light source; 6. Diffuser, green light filter and iris; 7. Photomacrographic zoom lens; 8. Video camera; 9. Computer with digitizer board; 10. Printer; 11. Plotter; 12. Black and white video monitor; 13. Ultra-stable table with 5, 6, 7 and 8 mounted on an optical rail; 14. Windows; 15. Liquid reservoir; 16. Anton Paar DMA 512 and 55 high-pressure density cell and digital readout; 17. Gas chromatograph; 18. Magnetic circulating pump; 19. 70 MPa pressure gauge graduated in 0.5 MPa intervals; 20. Two-stage gas compressor; 21. Methane gas cylinder; 22. To drain/vacuum; 23. Temperature controlled oven; 24/25. Temperature controllers for reservoir cell and lagged high-pressure lines; V1−V9. High-pressure valves. Dashed lines show electrical connections; dash/dotted lines represent thermostated control.
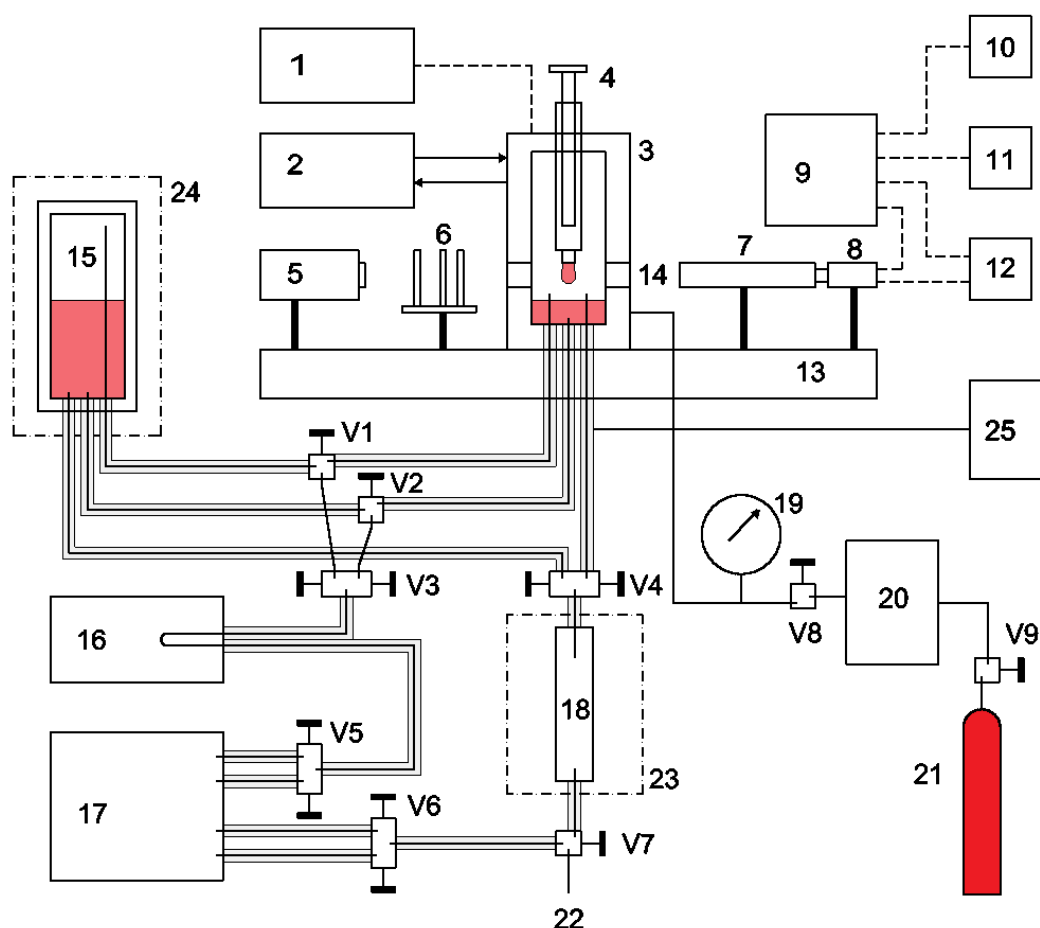
Fig. 3 (a) Drop profile coordinate system in the (X, Z) plane.[a] (b) Example of a Laplace-Young drop profile fitted to experimentally-acquired pendant drop profile coordinates.[b]

[a] (x, z) is a point on the drop profile, r is the radius of curvature at this point, ϕ is the angle between the horizontal and the tangent at point (x, z) and s is the arc length from the drop apex at $(0, 0)$ along the curve to point (x, z).

[b] Only 100 out of a total of 318 points have been plotted for this particular drop (as filled red circles) so that the curve through the points remains visible.
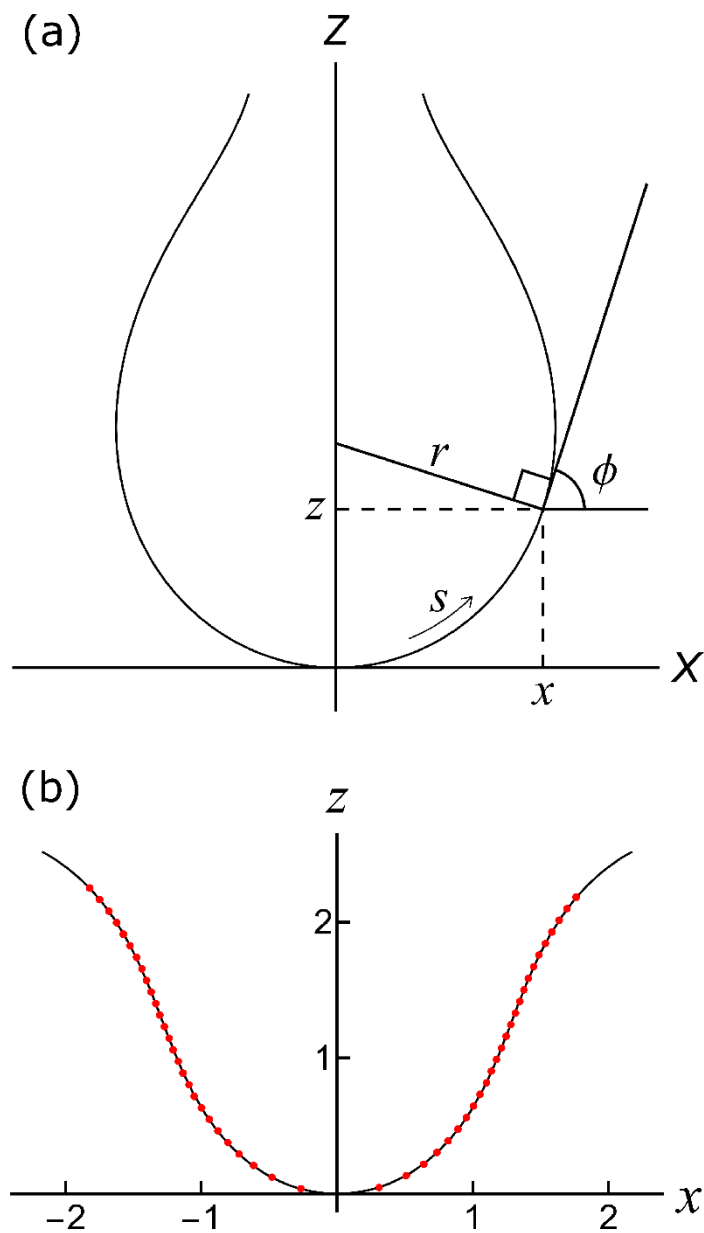
The set of differential equations (Eq. 1) can be integrated numerically using the Runge-Kutta method for a chosen value of β. This procedure generates the profile coordinates of a drop with unit radius of curvature at the apex, which is at (0, 0). By carrying out a non-linear least-square minimization between the experimentally-acquired profile coordinates and those generated from the Laplace-Young equation it is possible to find a value of β which gives a best fit to the data. This mapping process is achieved by introducing five free parameters corresponding to translations and scaling of the (x, z) set of coordinates, rotation (in case the camera is not vertically aligned), and scaling of the aspect ratio of the camera/lens system. An example of a set of experimentally-acquired drop profile coordinates is shown in Fig. 3b, together with a fitted profile curve that was determined in the manner just described. As can be seen, the quality of the fit is extremely good.

2.2. Gradient theory. The basic theory was first proposed in 1893 by van der Waals [28] and it was extended in 1958 by Cahn and Hilliard [29]. It has been described many times in the literature [30-40] and so we present here only an outline of our particular implementation of the approach. A central assumption is that the composition gradient is small compared with the reciprocal of the intermolecular distance. For a homogenous fluid at the same density as the real fluid, expansion of the Helmholtz free energy density a_0 as a (truncated) Taylor series [29] leads to Euler-Lagrange equations which, in the case of a planar surface perpendicular to z, can be simplified to

$$\sum_i \sum_j \kappa_{ij} \frac{\partial \rho_i}{\partial z} \frac{\partial \rho_j}{\partial z} = 2\, \Delta\Omega$$

(3)

in which ρ_i is the density of component i. In this expression, κ_{ij} is an element of the influence parameter matrix [41] which determines the density gradient response to the local deviation in the chemical potential from its bulk value [42]; it has been assumed in the derivation of Eq. 3 to vary only weakly with density. The quantity $\Delta\Omega$ is the change in the thermodynamic potential of the system, determined by

$$\Delta\Omega = a_0 - \sum_i \rho_i \mu_{i,s} + p_s$$

(4)

in which $\mu_{i,s}$ is the chemical potential of component i and p_s is the equilibrium pressure, where the subscript s denotes saturation conditions.

The calculation of the phase densities of an inhomogeneous fluid at saturation conditions requires an equation of state; the Peng-Robinson equation of state [43] has been widely used for this purpose because it gives good predictions of most phase properties. However, in the case of densities, particularly of the liquid phase, a volume shift [44] has been found to improve significantly the quality of the predicted values. The introduction of a volume shift transforms Eq. 3 to the following form:

$$\sum_i \sum_j \kappa_{ij} \frac{\partial \tilde{\rho}_i}{\partial z} \frac{\partial \tilde{\rho}_j}{\partial z} = 2 \Delta \tilde{\Omega}$$

(5)

in which the quantities with the ˜ accent are those which are modified by the volume shift (see Jaubert et al. [45]). In principle, the surface tension could be determined from

$$\gamma = \int_{-\infty}^{\infty} (2 \Delta \tilde{\Omega}) \, dz = \int_{-\infty}^{\infty} \left(\frac{\tilde{\rho}}{\rho} \right) (2 \Delta \Omega) \, dz$$

(6)

but in practice it turns out to be somewhat more straightforward to transform these expressions so as to be integrations over the density of one of the components, which we denote ρ_{ref}. Use of the chain rule, alongside Eq. 5, leads directly to

$$dz = \left(\frac{\tilde{\rho}}{\rho} \right)^{\frac{1}{2}} (2 \Delta \Omega)^{-\frac{1}{2}} \psi_{ref} \, d\rho_{ref}$$

(7)

in which we have defined

$$\psi_{ref} \equiv \left(\sum_i \sum_j \kappa_{ij} \frac{\partial \rho_i}{\partial \rho_{ref}} \frac{\partial \rho_j}{\partial \rho_{ref}} \right)^{\frac{1}{2}}$$

(8)

so that the surface tension can instead of Eq. 6 be determined from

$$\gamma = \int_{\rho_{ref}^V}^{\rho_{ref}^L} \left(\frac{\tilde{\rho}}{\rho} \right)^{\frac{3}{2}} (2 \Delta \Omega)^{\frac{1}{2}} \psi_{ref} \, d\rho_{ref}$$

(9)

The integration in Eq. 9 is along the path from ρ_{ref}^{V}, the density of component ref in the vapor, to ρ_{ref}^{L}, its corresponding density in the liquid phase. Assuming the usual geometric mixing rule for the influence parameters, $\kappa_{12} = \sqrt{\kappa_{11}\kappa_{12}}$, the integration along the path requires solving [40]:

$$\frac{\mu_{ref}(\rho_{ref}) - \mu_{ref,s}}{\sqrt{\kappa_{ref\ ref}}} = \frac{\mu_i(\rho_i) - \mu_{i,s}}{\sqrt{\kappa_{ii}}} \qquad \forall i$$

(10)

so as to find the $\{\rho_i\}$ that correspond to each chosen value of ρ_{ref} along the path.

Useful information is also provided by integrating Eq. 7:

$$\Delta z(\rho_{ref}) = \int_{\rho_{ref}^{V}}^{\rho_{ref}} \left(\frac{\tilde{\rho}}{\rho}\right)^{\frac{1}{2}} (2\,\Delta\Omega)^{-\frac{1}{2}} \psi_{ref}\, d\rho_{ref}$$

(11)

where the upper limit of integration, ρ_{ref}, is part way along the path from ρ_{ref}^{V} to ρ_{ref}^{L}. The resulting value of Δz goes from zero, when $\rho_{ref} = \rho_{ref}^{V}$ (i.e. bulk vapor), and it extends through the interfacial liquid/vapor region to bulk liquid, when $\rho_{ref} = \rho_{ref}^{L}$. Taken together with the $\{\rho_i\}$ obtained using Eq. 10, the outcome of this integration is the density profile of each component through the interfacial layer.

In the present work, dealing with the binary methane-pentane system, we chose ρ_{ref} to be ρ_2, i.e. the density of the n-pentane component. The justification for taking n-pentane as the reference component is presented later. For the volume shift, we used

$$\frac{\tilde{\rho}}{\rho} = \frac{1}{1 - \rho c}$$

(12)

where the value of c was chosen so that post processing of the Peng-Robinson equation of state flash calculations gave a good fit to the experimental liquid phase density data. Using also the geometric mixing rule (vide supra) for combining the influence parameters, Eqs. 9 and 11 simplify to the following:

$$\gamma = \int_{\rho_2^{V}}^{\rho_2^{L}} (1 - \rho c)^{-\frac{3}{2}} (2\,\Delta\Omega)^{\frac{1}{2}} \left(\sqrt{\kappa_{11}}\frac{d\rho_1}{d\rho_2} + \sqrt{\kappa_{22}}\right) d\rho_2$$

(13)

11

$$\Delta z(\rho_2) = \int_{\rho_2^V}^{\rho_2} (1 - \rho c)^{-\frac{1}{2}} (2\,\Delta\Omega)^{-\frac{1}{2}} \left(\sqrt{\kappa_{11}}\ \frac{d\rho_1}{d\rho_2} + \sqrt{\kappa_{22}} \right) d\rho_2$$

(14)

Individual alkane component data, together with various constants that were used in the Peng-Robinson equation of state, are listed in Table 2. The values of the binary interaction parameters that were used are $k_{11} = k_{22} = 1$ and $k_{12} = k_{21} = 0.98$ [46]. The influence parameters were taken as constant values along the density path of the homogeneous fluid at a given pressure, but were scaled by $(1 - p_s/p_c)$, where $p_c = 1.6 \times 10^7$ Pa is the critical pressure of the binary system, determined from the Wegner fit to the three experimental data sets (vide infra). The initial κ_{ii} values, determined by a least square fit of Eq. 13 to the experimental surface tension data, are 2.52×10^{-20} for methane and 3.29×10^{-19} for n-pentane (in $\mathrm{J\,m^{-5}\,mol^{-2}}$). These values are similar to those determined by Cornelisse [30].

The standard computational procedure that is normally used with gradient theory to determine surface tension is first to determine the density path and then to perform the integration along that path. For cases in which the determination of the path is time consuming, Larsen et al. [40] have proposed a method for significantly improving the overall computational speed, but retaining accuracy, by determining density values at a minimum number of knots such that the path is sufficiently well described by a spline. As alternatives to computing the path first, we considered simple schemes for accumulating the integral at the same time as determining the path, focusing instead on the minimum number of points that are required for the integrand. In particular, we found that an adaptive Simpson's ⅜ rule strategy provided highly accurate integrals with remarkably few intervals. The resulting values were compared with those obtained by carrying out the integration using instead the internal functions within Mathematica® [47], after determining the path.

For each saturation pressure, the Peng-Robinson equation of state was used to compute the inhomogeneous phase equilibrium properties and then to calculate the surface tension using the pre-calculated equilibrium phase densities. The temperature was fixed at 313.15 K with the pressure ranging from 0.5 to 15.6 MPa in steps of 0.01 MPa (*i.e.* 1511 steps). We found that it was not in fact necessary to compute the surface tension for all of these saturation pressures. Instead, it was sufficient to determine the surface tension at about twenty points and then to fit a spline through the data. This last simplification resulted in a significant speed up in the overall computational time (by a factor of *ca.* 140). Additionally, there is a trade-off between the step size and the speed of processing when doing the Peng-Robinson flash calculations. We found

that further reductions in the step size, so as to improve the convergence at the highest pressures, did not make any discernible difference to the calculated values of the surface tension at those pressures. All of the computational results presented here made use of Mathematica®.

Table 2. Properties of methane and *n*-pentane: critical temperature, critical pressure, molar critical volume, relative molar mass, acentric factor and molar volume translation.[a]

Substance	T_c / K	p_c / Pa	V_c / $m^3\,mol^{-1}$	RMM	ω	c / $m^3\,mol^{-1}$
methane	190.6	46.0×10^5	99.2×10^{-6}	16.043	0.011	-5×10^{-7}
n-pentane	469.7	33.7×10^5	31.3×10^{-5}	72.151	0.251	-5×10^{-6}

[a] Data taken from Reid et. al. [48] (methane) and Danesh [46] (*n*-pentane), except for the molar volume shift terms, determined by fitting by eye the Peng-Robinson liquid phase density.

2.3. Wegner scaling. Given that three different thermodynamic properties have been measured on the same system at the same time and at the same temperature, it is to be expected that they should extrapolate to a common critical pressure. Standard critical scaling relations of the form:

$$\gamma = \gamma_0 \, |p_r|^\nu$$

(15)

are not suitable for the present work because they theoretically only apply very close to the critical point, typically for reduced thermodynamic variables [49] less than 10^{-4} (where $p_r = |1 - p/p_c|$ is the reduced pressure, γ_0 is a system-dependent constant and ν is a universal exponent [50], equal to 1.26). Wegner [24] has derived the following extended scaling relationship using renormalization group techniques:

$$\gamma = p_r^\nu \sum_{n=0}^{\infty} \gamma_n \, p_r^{n\delta}$$

(16)

in which $\delta \approx 0.5$ is a universal 'gap' exponent. Eq. 16 applies over a much wider range of thermodynamic space than the standard critical scaling relations. Similar extended expressions can be derived for the density difference and for the composition and also for each limb of the

coexistence curve. Such expressions have terms that fall into three categories [51]: those that can be measured directly, those evaluated by theory, and those that can only be determined from fitting curves to experimental data. In general the critical pressure p_c belongs to the first category but may also be found using the third category; the scaling parameters such as v and δ belong to the second group, with best theoretical estimates [52, 53] being 1.26 and 0.5, respectively, whereas the remaining parameters and amplitudes can only be found by curve fitting.

To test this approach with the current sets of data we have treated each of the critical quantities as free parameters, namely critical pressure (p_c), critical density (ρ_c), critical composition (x_c) and all of the amplitudes. We used a Levenberg-Marquardt non-linear least-squares minimization scheme to fit all of the data in Table 3, so as to find a common critical pressure. This also enables best-fit curves to be drawn through each of the three different types of property that have been measured.

3. RESULTS AND DISCUSSION

Our experimental surface tension, density and composition data for the methane-pentane system are presented in Table 3 and they are depicted in Fig. 4a. The most comprehensive previous study of the phase and volumetric properties of this system is that by Sage et al. [54], who measured the specific volume of six mixtures of methane and n-pentane for seven different temperatures between 310.93 K and 510.93 K and at pressures up to 34.474 MPa. They interpolated their data graphically so as to find the specific volumes and compositions of the coexisting phases as a function of pressure at each of the temperatures they studied. Direct comparison of the present results with their measurements is not possible because they did not consider an isotherm at 313.15 K (310.93 K was the closest), but it was possible to interpolate their data so as to estimate the densities at 313.15 K. For each of the isotherms in Ref. [54], we firstly used a Wegner extended fit of their density data as a function of pressure, so that we could calculate the density (at each temperature) for all of the pressures in our study. Next we fitted polynomials to each of the isobars of the resulting density versus temperature data in order to calculate the density at 313.15 K. The results from these interpolations are included in Fig. 4a and, as can be seen, the comparison with the present data is very good. Incidentally, when doing these Wegner extended fits, it was observed that if the critical points estimated in Ref. [54] were included, the resulting plots of the dependence of the density on pressure do not have the characteristic 'flat' shapes usually found in the vicinity of the critical point. This

strongly suggests that the critical pressures are likely to have been overestimated by Sage et al. [54] and so these values were excluded from our fits.

Table 3. Experimental results[a] for the phase densities, phase compositions and surface tension in the methane–pentane system as a function of pressure at 313.15 K. Subscripts 1 and 2 refer to methane and n-pentane, respectively.

p / bar	Phase density / g cm^{-3}		Phase composition				γ / mN m^{-1}
			liquid		vapor		
			x_1	x_2	x_1	x_2	
11	0.5944	0.0167	0.048	0.952	0.823	0.177	12.0
26	0.5810	0.0272	0.101	0.899	0.886	0.114	10.13
51	0.5588	0.0400	0.181	0.819	0.923	0.077	7.61
76	0.5331	0.0593	0.263	0.737	0.925	0.075	5.37
101	0.5018	0.0862	0.351	0.649	0.918	0.082	3.26
126	0.4663	0.1160	0.430	0.570	0.896	0.104	1.68
142	0.4315	0.1514	0.501	0.499	0.871	0.130	0.761

[a] Standard uncertainties u are $u(p) = 0.5$ bar, $u(T) = 0.05$ K, $u(\text{density}) = 0.0002$ g cm^{-3}, $u(x) = 0.002$, and $u(\gamma) = 0.02$ mN m^{-1}.

Fig. 4   (a) Surface tension, phase density and phase composition in the methane-pentane system at 313.15 K as a function of pressure.[a] (b) Phase densities of the vapor and liquid methane-pentane system, with experimental values shown as filled red circles.[b]

[a] Filled symbols represent the liquid phase and open ones the vapor phase for density and composition results. The plus symbols are data for the coexisting phase densities obtained from Sage et al. [54] and open diamonds are surface tension data from Stegemeier and Hough [55] at 310.93 K. See text for the explanation of the curves drawn through the data points.

[b] The dashed curves are calculated from the Peng-Robinson equation of state while the continuous curves are for the volume-shifted Peng-Robinson equation of state.
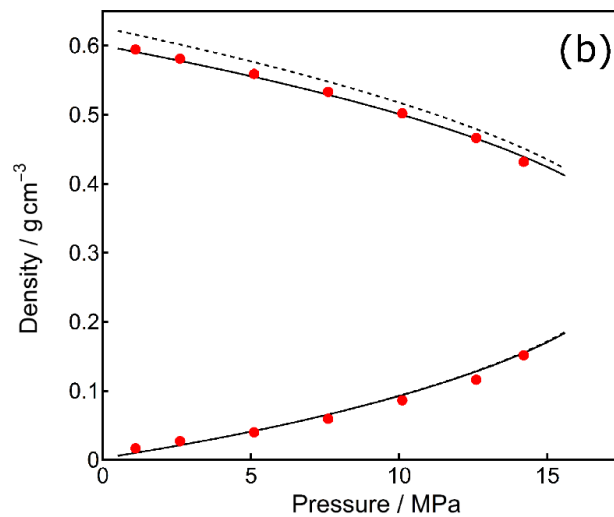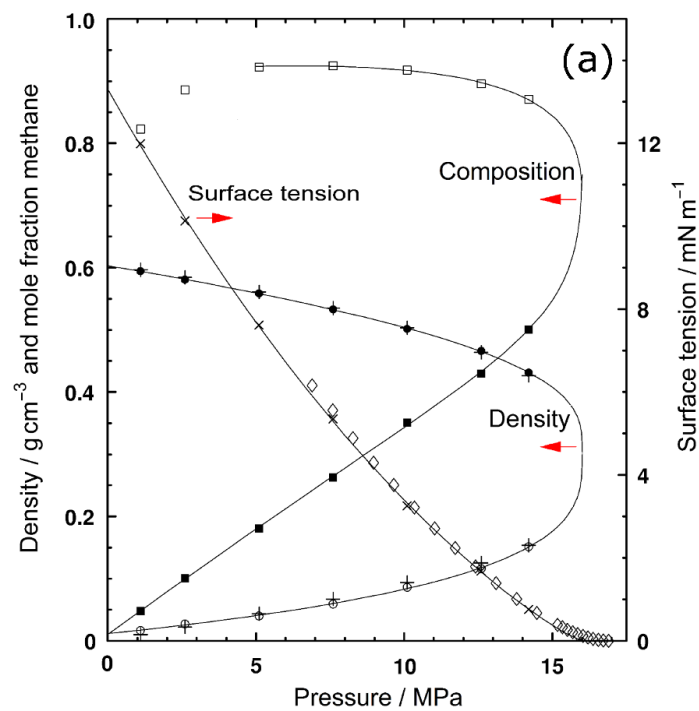
Stegemeier and Hough [55] have measured the surface tension of the methane-pentane system and so their results at 310.93 K are included in Fig. 4a, for the purposes of comparison. Our results are slightly below those in Ref. [55], as expected, due to the slightly lower temperature, but they do follow the same trend.

The curves drawn through the three sets of data points in Fig. 4a result from the Wegner fitting process described earlier and, as can be seen, the quality of the fit is very good. This strongly suggests that the Wegner extended scaling approach is ideally suited to estimating properties such as critical pressure, which are very difficult to measure experimentally. At pressures below about 5 MPa the composition has a negative pressure dependence, resulting in non-monotonic behavior that cannot easily be incorporated into the fitting process. Consequently, the two points at the lowest pressures have been excluded from the Wegner fits. The common critical pressure arising from our fitting process is 16 MPa, to be compared with the value of 16.93 MPa estimated by Sage et al. [54] for 310.93 K. As noted earlier, it is likely that they overestimated the critical pressures. Our value of 16 MPa for the critical pressure of the system at 313.15 K was used in the gradient theory approach to fit the influence parameters as a function of pressure.

Fig. 4b shows the experimental phase densities plotted against pressure together with the calculated values of the density using the Peng-Robinson equation of state, both with and without a volume translation. The volume translation makes essentially no difference for the vapor phase: the two curves are superimposed on one another. On the other hand, the liquid phase density is significantly overestimated by the Peng-Robinson equation of state but, with the introduction of a volume shift, the calculated densities compare very well with the measured values over the full pressure range.

The continuous curve in Fig. 5 indicates the surface tension calculated using Eq. 13, taking into account the volume shift (see Eq. 12), whereas the dashed curve corresponds to analogous calculations with $c = 0$. As is immediately apparent, the volume translation has a relatively small influence on the calculated surface tension, with the largest effect being at low pressure, but both sets of calculations tend towards the same values at the highest pressure. We note that qualitatively similar behavior for the effect of the volume translation on surface tension has been observed by Cornelisse for a range of binary systems [30].

Fig. 5   Surface tension as a function of pressure.[a]

[a] The two curves result from using gradient theory to compute the surface tension using Eq. 13 without (dashed curve) and with (continuous curve) the volume shift. Experimental results: filled red circles this work, filled black diamonds Amin et al. [56], filled black squares Stegemeier and Hough [55] and the filled black triangle on the *y*-axis Rios et al. [57].
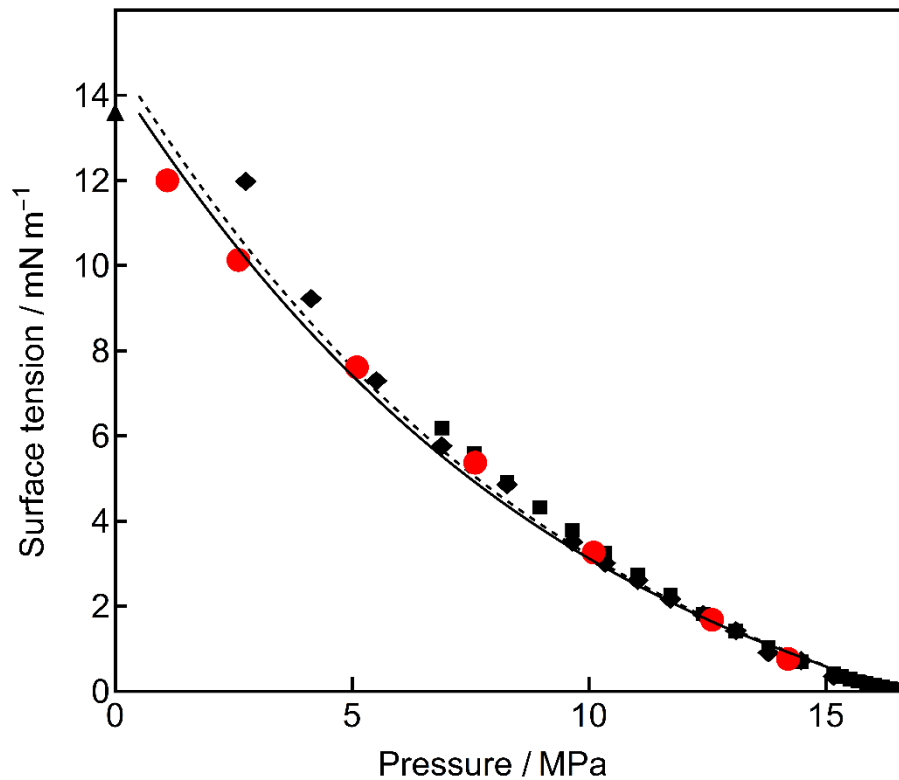
Our experimental data, together with other data sets, are also shown in Fig. 5. These data include the surface tension of *n*-pentane at saturation conditions [57] at 313.15 K (*i.e.* at 1.16 bar) [58]. As can be seen, the extrapolation through the data from this work tends towards this point, which is approximately where one would expect the surface tension of methane-pentane to be under those conditions. The data from Amin and Smith [56], while agreeing very well with our data at higher pressures, deviate to higher values of surface tension at the two lowest pressures. Their data are also inconsistent with the surface tension of *n*-pentane at 313.15 K under saturation conditions.

We mentioned earlier the need to justify taking the heavier component (*n*-pentane) as the reference component in the gradient theory approach to surface tension calculations. Confirmation that *n*-pentane was indeed the 'correct' choice is provided by an inspection of Fig. 6. Fig. 6a shows the homogeneous fluid having the same density as the heterogeneous system and is plotted as the density of methane against the density of *n*-pentane at three well separated isobars within the pressure range investigated. As can be seen, the density path is monotonically increasing with respect to the density of *n*-pentane for all three isobars. In other words, for a particular density of *n*-pentane there is only one corresponding density of methane, whereas for the converse this is not the case: there are two values of the *n*-pentane density for all methane densities, except at the maxima of the curves in Fig. 6a. Additionally, Fig. 6b shows the density profile of the two components across the interfacial region between the vapor and liquid phases for the same three isobars, calculated using Eq. 14. (The volume-shifted and $c = 0$ profiles turned out to be indistinguishable by eye.) As can be seen, the density of *n*-pentane (continuous curve) at the lowest of these isobars is a monotonic function of distance through the interface, whereas methane (broken curve) is preferentially adsorbed in the interfacial region, resulting in a density profile which has a maximum. The corresponding curves for the higher isobars follow the same trend, albeit within a decreasing interfacial thickness. These observations mean that in the calculations to determine the density path there will only be one solution with *n*-pentane as the reference, whereas if we had chosen methane much greater care would have been required to make sure that we found the correct solution. As such, the numerical root-finding process is much more straightforward if *n*-pentane is chosen as the reference component.

Fig. 6 (a) Density of methane against density of n-pentane (reference component) resulting from the solution to Eq. 10 and thereby specifying the density path at the isobars 0.5, 7 and 14 MPa; (b) Density profile of methane (dashed curve) and of n-pentane (continuous curve) through the surface region at the same isobars as in (a) calculated using Eq. 14 where c is the molar volume shift; (c) Variation of the integrand of Eq. 13 with n-pentane density for the same isobars as in (a) and (b).
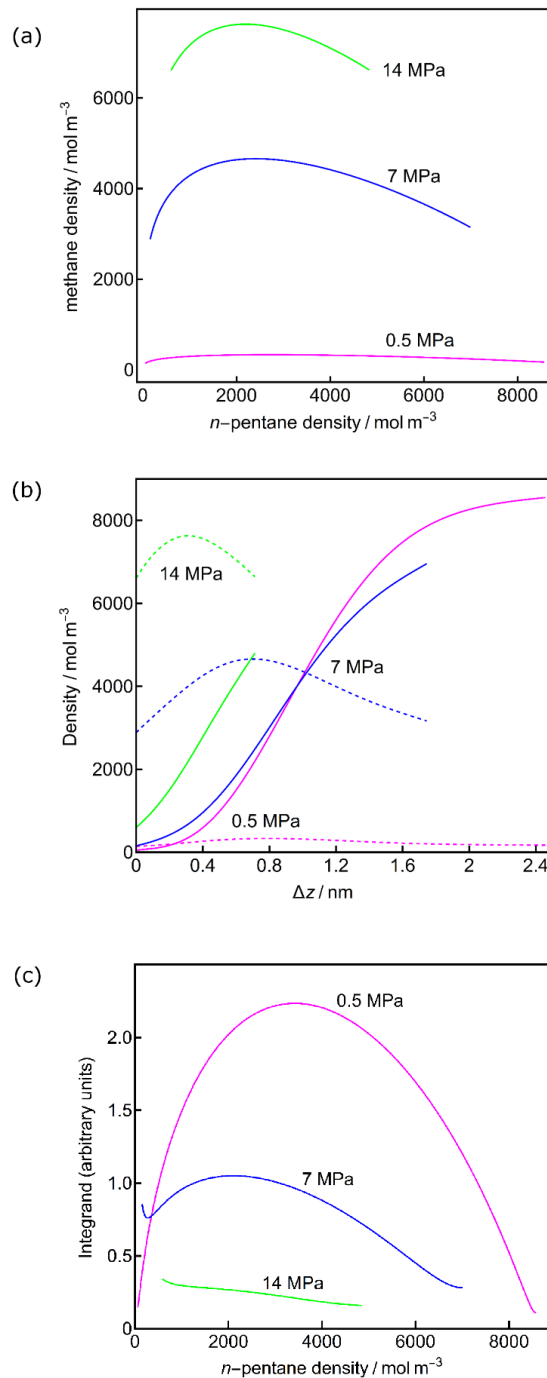
The calculation of the surface tension using Eq. 13 does of course involve finding the area under the curve generated by a particular integrand as a function of ρ_{ref}. Fig. 6c shows a plot of this integrand as a function of the *n*-pentane density for the same three isobars as in Fig. 6a and Fig. 6b. As can be seen, these curves are rather well behaved, making them very straightforward to integrate numerically using routines in Mathematica®. (Additionally this explains why our alternative approach, based on an adaptive Simpson's ⅜ rule, can deliver reliable surface tension data with such a small number of intervals across the ρ_{ref} coordinate.)

From critical scaling theory [53] it is found that thermodynamic properties such as surface tension or density difference scale in a universal way with variables such as reduced temperature or reduced pressure. These scaling relations can be expressed as in Eq. 15 for surface tension, where the exponent is equal to 1.26, and analogously for density difference, with instead a universal exponent equal to 0.325. Eliminating the reduced pressure from these two scaling relations leads to a direct relation between the surface tension and the density difference:

$$\gamma = c(\Delta\rho)^{3.88}$$

(17)

where c is a constant and the exponent is $3.88 = 1.26/0.325$. Schechter [59] has made a very good argument for using these scaling relations in preference to the parachor method when computing surface tension in fluids relevant to petroleum reservoirs. Given that we have estimated the critical pressure, it is a straightforward task to test these various scaling relations using our experimental data. Accordingly, surface tension and density difference have been plotted against reduced pressure in Fig. 7a and Fig. 7b, respectively, and they are plotted against each other in Fig. 7c. The straight lines shown in Fig. 7 are those predicted by the corresponding scaling relations and, as can easily be seen, the experimental data fit the theoretical predictions remarkably well. Of course the critical pressure was in fact determined by a fitting process using the experimental data. Nonetheless, the close match between the experimental data and the various scaling relations does indicate a high level of internal consistency in the data. An additional feature that is suggested by the level of agreement shown in Fig. 7 is that the higher order terms in the Wegner extended scaling approach must contribute a relatively small amount to the variables of interest for this system, over the range of conditions considered; otherwise, the data would not match so well the theoretical lines.

Fig. 7 Testing the scaling relations: (a) surface tension against reduced pressure; (b) density difference against reduced pressure; (c) surface tension against density difference. The lines shown in (a)-(c) correspond to the theoretical scaling relations, with gradients equal to 1.26, 0.325 and 3.88, respectively. Data from this study are shown as filled in red circles.
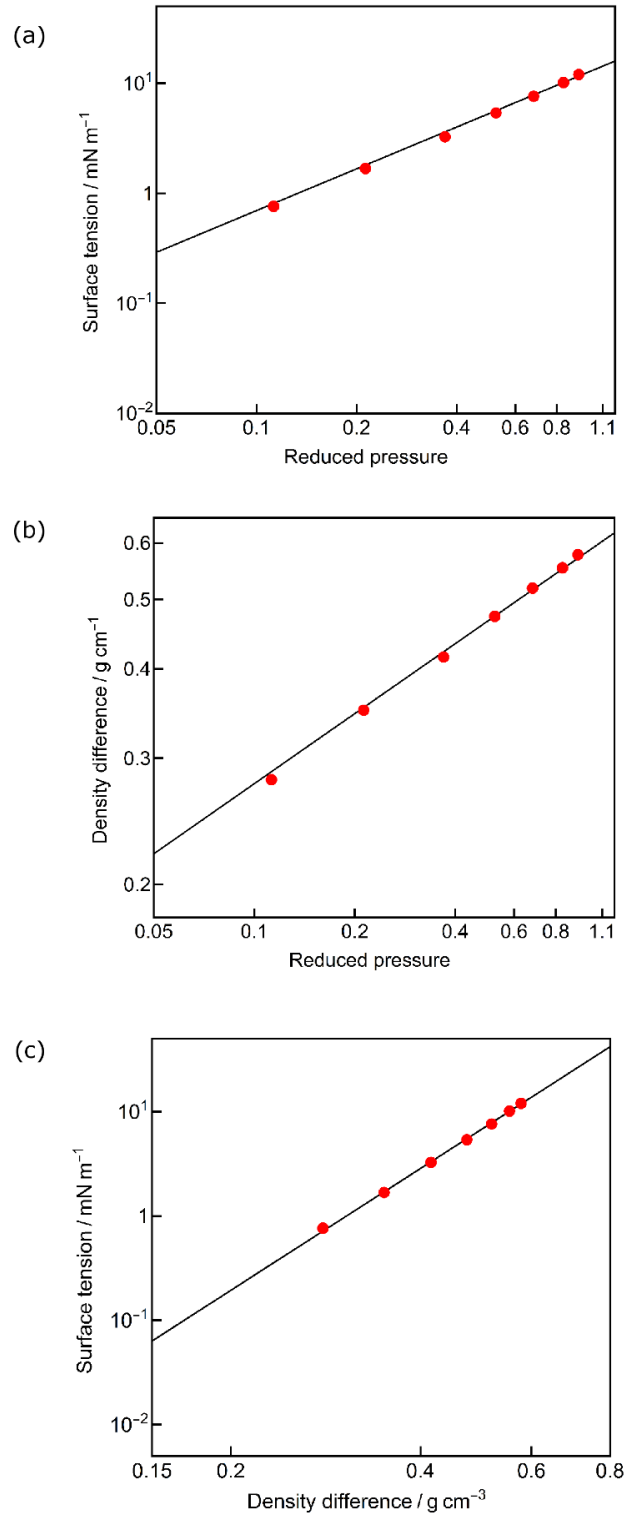
4. CONCLUSIONS

We have described new experimental apparatus that is well suited to the accurate measurement of surface tension and bulk thermodynamic properties in a system where miscibility changes very dramatically with changing pressure. It has been demonstrated that the apparatus works well for the methane-pentane system and that the resulting measurements compare well with literature data. Moreover it has also been demonstrated that a Wegner extended scaling approach enables the critical pressure to be estimated, using experimental data that are outside the critical range. Surface tension and density profiles calculated using the gradient theory approach are in very good agreement with the experimental data. Since both the comparison with literature data and the results from the theoretical calculations are extremely good we conclude that the experimental technique is validated. We now plan to utilize the combination of experimental and theoretical approaches described in this paper for various systems, including those relevant to enhanced oil recovery and for CO_2 sequestration in oil reservoirs that are out of production.
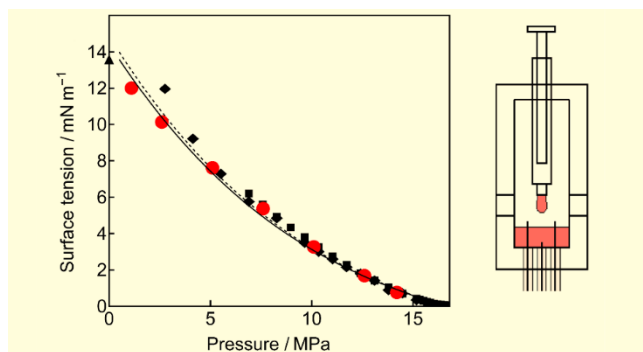
AUTHOR INFORMATION
Corresponding Author

*E-mail: js1@liverpool.ac.uk. Tel: +44 151 794 3530.
Notes

The authors declare no competing financial interest.

Table of Contents Only

REFERENCES

[1] W. Grochala, R. Hoffmann, J. Feng, N.W. Ashcroft, The Chemical Imagination at Work in Very Tight Places, Angew. Chem. Int. Ed., 46 (2007) 3620-3642.

[2] L. Zhang, Y. Wang, J. Lv, Y. Ma, Materials discovery at high pressures, Nat. Rev. Mater., 2 (2017) 17005.

[3] J.A. Torres, V. Serment-Moreno, Z.J. Escobedo-Avellaneda, G. Velazquez, J. Welti-Chanes, Reaction Chemistry at High Pressure and High Temperature, in: V.M. Balasubramaniam, G.V. Barbosa-Cánovas, H.L.M. Lelieveld (Eds.) Food Eng Ser, Springer New York, New York, NY, 2016, pp. 461-478.

[4] K. Yamamoto, Food processing by high hydrostatic pressure, Biosci. Biotechnol. Biochem., 81 (2017) 672-679.

[5] R. Bini, M. Ceppatelli, M. Citroni, V. Schettino, From simple to complex and backwards. Chemical reactions under very high pressure, Chem. Phys., 398 (2012) 262-268.

[6] A. Muggeridge, A. Cockin, K. Webb, H. Frampton, I. Collins, T. Moulds, P. Salino, Recovery rates, enhanced oil recovery and technological limits, Philos. Trans. R. Soc. London, Ser. A, 372 (2014) 20120320.

[7] J.L. Salager, A.M. Forgiarini, M.J. Rondon, How to Attain Ultralow Interfacial Tension and Three-Phase Behavior with a Surfactant Formulation for Enhanced Oil Recovery: a Review-Part 3. Practical Procedures to Optimize the Laboratory Research According to the Current State of the Art in Surfactant Mixing, J. Surfactants Deterg., 20 (2017) 3-19.

[8] K. Aziz, A. Settari, Petroleum Reservoir Simulation, Elsevier Applied Science Publishers, London, 1979.

[9] M. Shams, A.H. El-Banbi, M. Khairy, Effect of Capillary Pressure on the Numerical Simulation of Conventional and Naturally Fractured Reservoirs, North Africa Technical Conference and Exhibition, Society of Petroleum Engineers, Cairo, Egypt, 2013, SPE-164658-MS.

[10] B.A. Haider, K. Aziz, Impact of Capillary Pressure and Critical Property Shift due to Confinement on Hydrocarbon Production in Shale Reservoirs, SPE Reservoir Simulation Conference, Society of Petroleum Engineers, Montgomery, Texas, USA, 2017, SPE-182603-MS.

[11] J. Satherley, H.H.J. Girault, D.J. Schiffrin, The measurement of ultralow interfacial-tension by video digital- techniques, J. Colloid Interface Sci., 136 (1990) 574-580.

[12] E.A. Hauser, A.S. Michaels, Interfacial Tension at Elevated Pressures and Temperatures. I. A New and Improved Apparatus for Boundary-Tension Measurements by the Pendant-Drop Method, J. Phys. and Colloid Chem., 52 (1948) 1157-1165.

[13] J.M. Andreas, E.A. Hauser, W.B. Tucker, Boundary Tension of Pendant Drops, J. Phys. Chem., 42 (1938) 1001-1019.

[14] S. Fordham, On The Calculation of Surface Tension from Measurements of Pendant Drops, Proc. R. Soc. Lond. A., 194 (1948) 1-16.

[15] E.W. Hough, M.J. Rzasa, B.B. Wood, Interfacial Tensions at Reservoir Pressures and Temperatures; Apparatus and the Water-Methane System, Trans. AIME, 192 (1951) 57-60.

[16] M.E. Hassan, R.F. Nielson, J.C. Calhoun, Effect of pressure and temperature on oil-water interfacial tensions for a series of hydrocarbons, Pet. Trans. AIME, 198 (1953) 299-306.

[17] H.Y. Jennings, The Effect of Temperature and Pressure on the Interfacial Tension of Benzene-Water and Normal Decane-Water, J. Colloid Interface Sci., 24 (1967) 323-329.

[18] P. Fotland, A. Skauge, Ultralow Interfacial Tension as a Function Of Pressure, J. Dispersion Sci. Technol., 7 (1986) 563-579.

[19] P. Fotland, O.P. Bjørlykke, Phase Behaviour and Interfacial Tension as a Function of Pressure and Temperature in a Ternary Alkane System, J. Phys. Chem., 93 (1989) 6407-6413.

[20] M.S. Haniff, A.J. Pearce, Measuring Interfacial Tensions in a Gas-Condensate System With a Laser-Light-Scattering Technique, SPE Res. Eng., 5 (1990) 589-594.

[21] H.R. Zhang, B.J. Bjorkvik, B.J. Moffatt, Determination of Low Interfacial Tension with a Laser Light Scattering Technique and a Comparative Analysis With Drop Shape Methods, J. Colloid Interface Sci., 237 (2001) 11-20.

[22] L.M.C. Pereira, A. Chapoy, R. Burgass, B. Tohidi, Measurement and Modelling of High Pressure Density and Interfacial Tension of (Gas + n-Alkane) Binary Mixtures, J. Chem. Thermodyn., 97 (2016) 55-69.

[23] J.P. Millette, D.S. Scott, I.G. Reilly, P. Majerski, J. Piskorz, D. Radlein, T.J.W. deBruijn, An Apparatus for the Measurement of Surface Tensions at High Pressures and Temperatures, Can. J. Chem. Eng., 80 (2002) 126-134.

[24] F.J. Wegner, Corrections to Scaling Laws, Phys. Rev. B, 5 (1972) 4529-4536.

[25] L. Haar, J.S. Gallagher, G.S. Kell, NBS/NRC Steam Tables: Thermodynamic and Transport Properties and Computer Programs for Vapor and Liquid States of Water in SI Units, Hemisphere, Washington, 1984.

[26] S. Angus, K.M. de Reuck, International Thermodynamic Tables of the Fluid State, Helium-4, Pergamon Press, Oxford, 1977.

[27] H.H.J. Girault, D.J. Schiffrin, B.D.V. Smith, The Measurement of Interfacial Tension of Pendant Drops Using a Video Image Profile Digitizer, J. Colloid Interface Sci., 101 (1984) 257-266.

[28] J.S. Rowlinson, Translation of J. D. van der Waals' "The Thermodynamic Theory of Capillarity Under the Hypothesis of a Continuous Variation of Density", J. Stat. Phys., 20 (1979) 197-244.

[29] J.W. Cahn, J.E. Hilliard, Free Energy of a Nonuniform System. I. Interfacial Free Energy, J. Chem. Phys., 28 (1958) 258-267.

[30] P.M.W. Cornelisse, The Square Gradient Theory Applied-Simultaneous Modelling of Interfacial Tension and Phase Behaviour, PhD Thesis, TU Delft, 1997.

[31] P.M.W. Cornelisse, C.J. Peters, J.D. Arons, Simultaneous Prediction of Phase-Equilibria, Interfacial-Tension and Concentration Profiles, Mol. Phys., 80 (1993) 941-955.

[32] P.M.W. Cornelisse, C.J. Peters, J.D. Arons, Application of the Peng-Robinson Equation of State to Calculate Interfacial-Tensions and Profiles at Vapor-Liquid Interfaces, Fluid Phase Equilib., 82 (1993) 119-129.

[33] P.M.W. Cornelisse, C.J. Peters, J.D. Arons, On The Fundamentals of the Gradient Theory of van der Waals, J. Chem. Phys., 106 (1997) 9820-9834.

[34] C. Miqueu, B. Mendiboure, A. Graciaa, J. Lachaise, Modelling of the Surface Tension of Pure Components With the Gradient Theory of Fluid Interfaces: A Simple and Accurate Expression for the Influence Parameters, Fluid Phase Equilib., 207 (2003) 225-246.

[35] C. Miqueu, B. Mendiboure, A. Graciaa, J. Lachaise, Modeling of the Surface Tension of Multicomponent Mixtures With the Gradient Theory of Fluid Interfaces, Ind. Eng. Chem. Res., 44 (2005) 3321-3329.

[36] C. Miqueu, B. Mendiboure, C. Graciaa, J. Lachaise, Modelling of the Surface Tension of Binary and Ternary Mixtures With the Gradient Theory of Fluid Interfaces, Fluid Phase Equilib., 218 (2004) 189-203.

[37] A.J. Queimada, C. Miqueu, I.M. Marrucho, G.M. Kontogeorgis, J.A.P. Coutinho, Modeling Vapor-Liquid Interfaces With the Gradient Theory in Combination With the CPA Equation of State, Fluid Phase Equilib., 228 (2005) 479-485.

[38] A. Mejía, H. Segura, M. Cartes, J.R. Pérez-Correa, Experimental Determination and Theoretical Modeling of the Vapor-Liquid Equilibrium and Surface Tensions of Hexane plus Tetrahydro-2H-Pyran, Fluid Phase Equilib., 316 (2012) 55-65.

[39] H. Lin, Y.Y. Duan, Q. Min, Gradient Theory Modeling of Surface Tension for Pure Fluids and Binary Mixtures, Fluid Phase Equilib., 254 (2007) 75-90.

[40] P.M. Larsen, B. Maribo-Mogensen, G.M. Kontogeorgis, A Collocation Method for Surface Tension Calculations With the Density Gradient Theory, Fluid Phase Equilib., 408 (2016) 170-179.

[41] V. Bongiorno, L.E. Scriven, H.T. Davis, Molecular Theory of Fluid Interfaces, J. Colloid Interface Sci., 57 (1976) 462-475.

[42] B.S. Carey, L.E. Scriven, H.T. Davis, Semi-Empirical Theory of Surface Tensions of Pure Normal Alkanes and Alcohols, AIChE J., 24 (1978) 1076-1080.

[43] D. Peng, D.B. Robinson, New 2-Constant Equation of State, Ind. Eng. Chem. Fundam., 15 (1976) 59-64.

[44] A. Péneloux, E. Rauzy, R. Fréze, A Consistent Correction for Redlich-Kwong-Soave Volumes, Fluid Phase Equilib., 8 (1982) 7-23.

[45] J.N. Jaubert, R. Privat, Y. Le Guennec, L. Coniglio, Note on the Properties Altered by Application of a Péneloux-type Volume Translation to an Equation of State, Fluid Phase Equilib., 419 (2016) 88-95.

[46] A. Danesh, PVT and Phase Behaviour of Petroleum Reservoir Fluids, Elsevier, Amsterdam, 1998.

[47] Wolfram Research, Inc., Mathematica, Version 11.1, Wolfram Research, Inc., Champaign, Illinois, 2017.

[48] R.C. Reid, J.M. Prausnitz, B.E. Poling, The Properties of Gases and Liquids, 4th ed., McGraw-Hill, New York, 1987.

[49] J.V. Sengers, J.M.H. Levelt Sengers, Thermodynamic Behaviour of Fluids Near the Critical Point, Annu. Rev. Phys. Chem., 37 (1986) 189-222.

[50] B. Widom, Surface Tension and Molecular Correlation Near the Critical Point, J. Chem. Phys., 43 (1965) 3892-3897.

[51] J.-M. Barbarin-Castillo, I.A. McLure, The Orthobaric Coexisting Densities of $\{x\mathrm{Si(CH_3)_4} + (1-x)\mathrm{C(CH_3)_4}\}$ from $T \approx 360$ K up to the Gas-Liquid Critical Line: A Possible Experimental Route for the Verification of the Lorentz or Arithmetic-Mean Combining Rule for Mixtures of Quasi-Spherical Molecules, J. Chem. Thermodyn., 29 (1997) 1417-1434.

[52] J.S. Le Guillou, J. Zinn-Justin, Critical Exponents From Field Theory, Phys. Rev. B, 21 (1980) 3976-3998.

[53] J.S. Rowlinson, B. Widom, Molecular Theory of Capillarity, Clarendon Press, Oxford, 1982.

[54] B.H. Sage, H.H. Reamer, R.H. Olds, W.N. Lacey, Phase Equilibria in Hydrocarbon Systems: Volumetric and Phase Behavior of methane−n-pentane system, Ind. Eng. Chem., 34 (1942) 1108-1117.

[55] G.L. Stegemeier, E.W. Hough, Interfacial Tension of the Methane−n-Pentane System, Prod. Monthly, 25 (1961) 6-9.

[56] R. Amin, T.N. Smith, Interfacial Tension and Spreading Coefficient Under Reservoir Conditions, Fluid Phase Equilib., 142 (1998) 231-241.

[57] R. Rios, J. Ortega, L. Fernandez, I. de Nuez, J. Wisniak, Improvements in the Experimentation and the Representation of Thermodynamic Properties (iso-p VLE and y^E) of Alkyl Propanoate + Alkane Binaries, J. Chem. Eng. Data, 59 (2014) 125-142.

[58] A.P. Froba, L.P. Pellegrino, A. Leipertz, Viscosity and Surface Tension of Saturated n-pentane, Int. J. Thermophys., 25 (2004) 1323-1337.

[59] D.S. Schechter, B. Guo, Parachors based on modern physics and their uses in IFT prediction of reservoir fluids, SPE Reservoir Eval. Eng., 1 (1998) 207-217.